JOURNAL OF AIRCRAFT
Vol. 36, No. 4, July–August 1999

Finite Element-Based Analytic Shape Sensitivities of Local and Global Airframe Buckling Constraints

Youngwon Shin* and Eli Livne†
University of Washington, Seattle, Washington 98195-2400

An examination of available shell finite elements suitable for buckling analysis of thin-walled airframe structures leads to the selection of a simple, accurate, design-oriented element, which is then used with slight modifications to obtain explicit, closed-form equations for the stiffness and geometric stiffness matrices. In turn, these equations are used to derive explicit expressions for the analytic sensitivities of stiffness and geometric stiffness matrices with respect to shell shape design variables. With analytic shape sensitivities of structural matrices and corresponding buckling eigenvalues at hand, the resulting new computer capability makes it possible to construct buckling constraint approximations for approximation-concepts-based structural synthesis, as well as to examine sources of numerical noise that might appear when parametric studies or finite difference sensitivities are carried out using existing finite element codes. The simplicity of the shell elements used and the elimination of the need to carry out numerical integration lead to computational savings, especially when repetitive analyses have to be carried out during shape design optimization of typical airframes. The new capability is aimed at capturing both local and global modes of buckling failure with the same finite element model. Subcomponent interaction during buckling can, thus, be taken into account during shape optimization of wing and fuselage structures. Numerical tests involving plates, thin-walled channel sections, and a complete wing box of a typical fighter airplane demonstrate the effectiveness and accuracy of the new design-oriented capability.

Nomenclature

A	= area of triangular element
$[A]$	= a transformation matrix [see Eqs. (26), (27), (A1)]
a	= cross-sectional width of channel
b	= cross-sectional height of channel
$[D]$	= constitutive matrix [Eqs. (9), (35)]
E	= Young's modulus
$\{\boldsymbol{f}\}$	= consistent load vector
$\{\boldsymbol{G}\}, \{\boldsymbol{H}\}$	= direction vectors determining element orientation in global axes [Eq. (45)]
h	= layer thickness
J	= transformation Jacobian from physical to area coordinates
K	= buckling coefficient, Eq. (89)
$[K]$	= stiffness matrix
$[K_G]$	= geometric stiffness matrix
$\lfloor \boldsymbol{L} \rfloor$	= row vector of generalized coordinates used for the transverse shear fields over an element [Eq. (24)]
$\{\boldsymbol{l}\}, \{\boldsymbol{m}\}, \{\boldsymbol{n}\}$	= direction vectors determining element orientation in global axes [Eq. (47)]
$\{M\}$	= bending moment
$\lfloor N \rfloor$	= row vector of displacement shape functions [Eq. (5)]
N_x, N_y, N_{xy}	= in-plane loads in an element under static load
$\boldsymbol{n}$	= vector direction along a side of the triangle
$\{\boldsymbol{P}\}$	= static load vector
$[R], [S]$	= matrices used in the decomposition of element-bending stiffness matrix, see Eqs. (38), (39)
s	= direction perpendicular to the side of the triangle
$[T]$	= geometric transformation matrix from local to global coordinates [Eq. (46)]
t	= wall thickness
u	= x displacement in local coordinates
v	= y displacement in local coordinates
w	= z displacement in local coordinates
X_i, Y_i, Z_i	= coordinates of node i in global axes
x_2, x_3, y_3	= shape design variables of triangular element in local coordinates
β	= transverse shear angle
$\{\boldsymbol{\delta}\}$	= vector of degrees of freedom
ε	= strains
$\zeta_1, \zeta_2, \zeta_3$	= area coordinates
$[\Lambda]$	= geometric transformation matrix from local to global coordinates [Eq. (55)]
λ	= buckling eigenvalue
σ	= stresses
ϕ	= eigenvector
Ψ	= node locations in global coordinates
ψ	= node locations in local coordinates

Superscripts and Subscripts

b	= bending action
cr	= critical
e	= related to an element
m	= membrane action
n	= vector direction along a side of the triangle
s	= direction perpendicular to the side of the triangle
x, y	= x and y directions in local coordinates

Introduction

BUCKLING of thin-walled structures is one of the most important structural failure modes considered and controlled during design synthesis of flight vehicles. Typically, in the case of conventional airframes, buckling analysis of skin and fuselage panels is carried out under the assumption that individual panels (whether flat or curved) buckle independently of each other. In most cases during preliminary design (where discrete point supports using rivets or spot welding are still too detailed to be considered), boundary conditions for buckling analysis of individual panels are taken to be simply supported. This represents a conservative approach facing the uncertainty associated with precise simulation of the flexibility

Received 7 October 1997; revision received 15 December 1998; accepted for publication 6 February 1999.

*Graduate Student, Department of Aeronautics and Astronautics.
†Associate Professor, Department of Aeronautics and Astronautics. eli@aa.washington.edu. Associate Fellow AIAA.

of edge supports contributed by the panel's connections to adjoining panels as well as by stringers, frames, ribs, and spars, which surround the panel.

In the context of structural optimization in a typical evaluation of linear buckling constraints, stress analysis of the entire airframe will be usually followed by buckling analyses of buckling-critical individual panels. Dependence of buckling constraints on sizing type design variables can be complex and quite nonlinear because local variation of panel structural designs will affect not only the panels themselves, but also the stress distribution in the complete structure. The same happens when airframe shape design variables are considered—an important phase during conceptual design, where the shape of an aircraft is to be synthesized. Variation of overall shape design variables such as wing sweep or aspect ratio affects stress distribution under load, but also affects the shape of individual panels, as spars and ribs change positions correspondingly. Panels that start by belonging to the buckling-critical set of panels at the outset of the design process might become noncritical, whereas other panels, not initially included in this set, might become critical as the design evolves. Moreover, strong interactions among neighboring panels or among panels and webs of supporting ribs and spars can arise as a configuration might change shape significantly compared to its initial design. A design-oriented analysis capability, including automatic mesh generation and mesh variation as well as behavior sensitivities and approximations and which can effectively track modes of buckling failure during the sizing/shape optimization of airframes, is, thus, highly desirable.

Numerous references published over the last 30 years address the problems of panel-buckling optimization and the interplay between the local buckling optimization of individual panels and the global optimization of the complete airframe.[1–10] Research efforts to examine the significance of global buckling analysis in airframe structural optimization (allowing for subcomponent interactions during buckling) had been scarce[11,12] and were limited to sizing type-design variables and to structural configurations made of rectangular subcomponents. Of course, any finite element-based buckling-analysis capability can be used for shape optimization if behavior sensitivities are calculated by finite differences or by semianalytic differentiation. However, the computational cost and numerical problems associated with finite differences are well known[13] as are potential accuracy problems associated with the semianalytic method. Research efforts to develop design-oriented structural modeling techniques with analytic shape sensitivities for airframe shape optimization had been very scarce too,[14–17] even though structural shape optimization is a well-established technology, applied successfully to many design synthesis problems in the car, ship, machine-part, and civil engineering industries.[18–25]

In Ref. 26 a design-oriented skin buckling analysis for shape optimization of wing structures was presented, taking into account the local and global effects of variations in panel design variables, addressing skin panels of general trapezoidal planform, but still limited to single panels simply supported on all edges. The present article presents a finite element-based design-oriented airframe buckling analysis capable of predicting buckling modes involving interactions among subcomponents as well as buckling of single stiffened panels, with geometric configurations made of general trapezoidal segments. Although this type of *analysis* can be carried out today with general purpose finite element codes,[12] the new capability presented here includes *sensitivities* of buckling constraints (with respect to panel and overall shape design variables) obtained *analytically* and *explicitly*.

As the present article shows, careful selection of the shell elements used in the new design-oriented airframe structural analysis capability makes it possible to obtain stiffness and geometric stiffness matrices as well as their sensitivities with respect to shape in closed form and without the use of numerical quadrature. There are significant computational gains associated with the increased speed with which element matrices are calculated using this explicit, closed-form formulation. The paper reviews the equations used to generate stiffness and geometric stiffness matrices and then moves on to describe calculation of analytic sensitivities of these matrices with respect to sizing and shape design variables, leading to sensitivities of the buckling eigenvalues themselves. Test cases involving plates, thin-walled channels, and a realistic fighter wing structure are used to assess computational effectiveness; accuracy and convergence of the buckling analysis; successful capturing of buckling modes involving subcomponent interactions; and sources of numerical noise in parametric results, as well as accuracy of the sensitivity analysis and associated approximations. The resulting capability is constructed for integration with nonlinear programming/approximation concepts (NLP/AC) based structural optimization.[27]

Linear Strain Discrete Kirchhoff Flat Shell Triangular Element with Loof Nodes

When searching for a design-oriented shell element, for airframe stress and buckling analysis, the following features are sought: 1) the element should be simple to formulate, with explicit equations that can be used to obtain analytic sensitivities with respect to shape, material, and sizing design variables; 2) the element should be reliable and capable of capturing accurately the stress and buckling behavior of typical wing and fuselage structures; 3) the element should be computationally efficient, an important consideration in any optimization capability where repetitive evaluation of structural behavior is required; and 4) it should be possible, using the selected element, to model shell, plate, and any thin-walled built-up structure of general shape, including structures with sharp fold lines or with multiple surfaces meeting at joint lines (such as when spar or rib webs in a wing meet the upper or lower skins).

An examination of the large number of shell elements developed over the years[24,28–30] shows that the flat triangular shell element of Refs. 31–33 meets all of the requirements just stated. Unlike most curved shell elements, which lead to quite complex formulation and numerically expensive evaluation of their stiffness and geometric stiffness matrices, this flat element is simple, and its formulation can be done explicitly in closed form. It avoids many of the difficulties associated with other flat shell elements such as the problems with drilling degrees of freedom, or the inconsistent displacement fields used to describe in-plane and transverse behavior.[30,34–41] The geometric inaccuracies caused by the approximation of the structure by a mesh of flat facets are not very severe in the case of typical wing structures, where curvature of the skins is usually moderate. In the case of fuselage structures, the element is expected to perform accurately as well (as Ref. 17 demonstrates using flat shell elements and as Ref. 32 shows in the cases of cylindrical roof and a pinched cylinder).

Detailed derivation, adopting a design-oriented perspective, of structural matrices for the element in local and global coordinates, is presented in the following sections. All major assumptions are summarized, and the resulting equations (expressed explicitly in terms of design variables) are cast in a form that makes application of automated symbolic algebra straightforward.

Element Geometry in Local Axes

As Fig. 1 shows, the element is positioned in local x, y axes so that its 1-2 side is along the x axis and vertex 1 is at the origin.

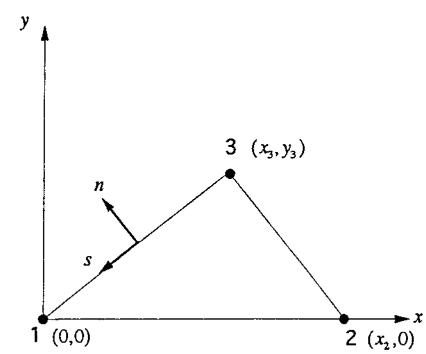

Fig. 1 Element shape design variables and vector side directions (n, s) in local axes.

Out of the six vertex coordinates defining the shape of the element, only three are necessary: x_2, x_3, and y_3 because $x_1 = y_1 = y_2 = 0$. Area coordinates $\zeta_1, \zeta_2, \zeta_3$ are used in the derivation of stiffness and geometric stiffness equations.[30,42] The area of the element is

$$A = \tfrac{1}{2} x_2 y_3$$

Exact-area integration formulas, which are used extensively in the derivation of element matrices, are, thus, explicitly dependent on element shape design variables (vertex coordinates):

$$\iint_A \zeta_1^a \zeta_2^b \zeta_3^c \, dA = \frac{a!b!c!}{(a+b+c+2)!} 2A = \frac{a!b!c!}{(a+b+c+2)!} x_2 y_3$$

Six nodes (the vertices 1, 2, 3) and the midside nodes (4, 5, 6) as well as six Loof nodes (i–vi) are used. With nodes 4–6 located in the middle of the sides, and when independent local coordinates ξ_1, ξ_2 ae used, it is possible to get explicit inverse-Jacobian as

$$\begin{bmatrix} \dfrac{\partial \xi_1}{\partial x} & \dfrac{\partial \xi_2}{\partial x} \\ \dfrac{\partial \xi_1}{\partial y} & \dfrac{\partial \xi_2}{\partial y} \end{bmatrix} = \frac{1}{J} \begin{bmatrix} -y_3 & y_3 \\ x_3 - x_2 & x_3 \end{bmatrix}$$

where

$$J = 2A = x_2 \cdot y_3 \tag{1}$$

and integration of a polynomial in area coordinates over the triangle area is accomplished by the following formula:

$$\int_0^1 \int_0^{1-\xi_1} \xi_1^m \xi_2^n \, d\xi_2 \, d\xi_1 = \frac{m!n!}{(2+m+n)!} \tag{2}$$

The Loof nodes are located at Gaussian points on each side.[30] Expressing x, y positions of all nodes explicitly in terms of the element's shape design variables x_2, x_3, and y_3 is straightforward because the transformation of a point $\omega = \pm 0.57735026919$, $\omega \in [-1, 1]$ to a corresponding point on any side connecting (x_i, y_i) and (x_j, y_j) is

$$x = [(1-\omega)/2]x_i + [(1+\omega)/2]x_j$$
$$y = [(1-\omega)/2]y_i + [(1+\omega)/2]y_j \tag{3}$$

where $\omega = 0$ for the midpoints 4, 5, 6 and where the two Loof nodes on each side correspond to $\omega = \pm 0.57735026919$.

Membrane Action

The Linear Strain Triangle (LST) is used for modeling membrane behavior of the shell because of its good convergence properties in plane stress cases[15,43] and because of its quadratic displacement field. This in-plane quadratic displacement field is consistent with the quadratic transverse displacement field used to model bending, as is shown in the following section. Design-oriented formulation of the equations for LST stiffness matrices, leading to explicit expressions in terms of sizing type and shape design variables as well as analytic sensitivities with respect to sizing, material, and shape design variables, are described in Refs. 15, 17, and 44. A different, more general, approach is taken here and is used for formulation of bending stiffness and geometric stiffness as well. In the following the principles and the equations used to obtain such explicit formulations are described in a self-contained manner. Detailed derivations can be found in the references.

The in-plane x and y displacements are quadratic over an element.

$$u = \lfloor N \rfloor \{u^m\}, \qquad v = \lfloor N \rfloor \{v^m\} \tag{4}$$

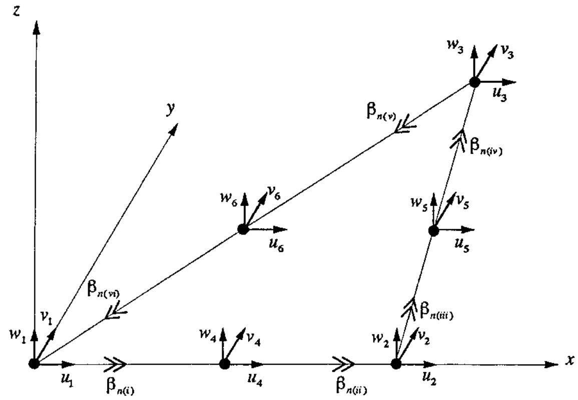

Fig. 2 Element translational and rotational degrees of freedom.

where

$$\lfloor N \rfloor = \lfloor \zeta_1(2\zeta_1 - 1) \;\; \zeta_2(2\zeta_2 - 1) \;\; \zeta_3(2\zeta_3 - 1) \;\; 4\zeta_1\zeta_2 \;\; 4\zeta_2\zeta_3 \;\; 4\zeta_1\zeta_3 \rfloor \tag{5}$$

The u, v displacements at nodes 1–6 (Fig. 2) are

$$\{u^m\} = \{u_1, u_2, u_3, u_4, u_5, u_6\}, \qquad \{v^m\} = \{v_1, v_2, v_3, v_4, v_5, v_6\} \tag{6}$$

leading to membrane strains

$$\{\varepsilon^m\}^T = \left\{ \varepsilon_{xx}^m \quad \varepsilon_{yy}^m \quad \gamma_{xy}^m \right\}$$

$$\{\varepsilon^m\} = \begin{Bmatrix} \lfloor N,_x \rfloor & \lfloor 0 \rfloor \\ \lfloor 0 \rfloor & \lfloor N,_y \rfloor \\ \lfloor N,_y \rfloor & \lfloor N,_x \rfloor \end{Bmatrix} \begin{Bmatrix} \{u^m\} \\ \{v^m\} \end{Bmatrix} = [B^m] \begin{Bmatrix} \{u^m\} \\ \{v^m\} \end{Bmatrix} \tag{7}$$

The corresponding membrane forces $\{N_x, N_y, N_{xy}\}^T$ are

$$\{N\} = [D_m]\{\varepsilon^m\} \tag{8}$$

where, for isotropic material with thickness t, Young's Modulus E, and Poisson's ratio ν,

$$[D_m] = \begin{bmatrix} \dfrac{Et}{(1-\nu^2)} & \dfrac{\nu Et}{(1-\nu^2)} & 0 \\ \dfrac{\nu Et}{(1-\nu^2)} & \dfrac{Et}{(1-\nu^2)} & 0 \\ 0 & 0 & \dfrac{Et}{2(1+\nu)} \end{bmatrix} \tag{9}$$

The element membrane stiffness matrix becomes

$$[K^m] = \iint_A [B^m]^T [D_m][B^m] \, dA \tag{10}$$

where $[B^m]$ is defined in Eq. (7) and is expressed explicitly in terms of local area coordinates and element shape design variables using

$$\lfloor N,_x \rfloor = \frac{1}{J} \begin{Bmatrix} -y_3(4\xi_1 - 1) \\ y_3(4\xi_2 - 1) \\ 0 \\ 4(-y_3\xi_2 + y_3\xi_1) \\ 4y_3\xi_3 \\ -4y_3\xi_3 \end{Bmatrix}^T$$

$$\lfloor N,_y \rfloor = \frac{1}{J}\begin{Bmatrix} -(x_2-x_3)(4\xi_1-1) \\ -x_3(4\xi_2-1) \\ x_2(4\xi_3-1) \\ 4[-x_3\xi_1-(x_2-x_3)\xi_2] \\ 4(-x_3\xi_3+x_2\xi_2) \\ -4[(x_2-x_3)\xi_3-x_2\xi_1] \end{Bmatrix}^T \tag{11}$$

Substitution of Eqs. (7), (9), and (11) into Eq. (10) gives

$$[K^m] = (1/J)[\bar{K}^m] \tag{12}$$

where

$$[\bar{K}^m] = \iint_A [B^m]^T[D_m][B^m]J\,\mathrm{d}A \tag{13}$$

Each element of $[K^m]$ is, then, a linear combination of integrals of the type shown in Eq. (2). Each contributing term of the form constant $\times \iint_A \zeta_1^a\zeta_2^b\zeta_3^c\,\mathrm{d}A$ is, then, evaluated analytically. The triple product in the integrand of Eq. (10) can be carried out manually. However, the tedious evaluation of this triple product explicitly in terms of shape design variables ($x2$, $x3$, $y3$) and monomials in area coordinates can be carried out automatically using symbolic equation manipulators.[45–49] In the case of this work, the Mathematica code[50] was used. The resulting stiffness matrix representing membrane behavior depends explicitly on the thickness, material, and shape design variables. In the case of composite laminates, the constitutive matrix $[D_m]$ is obtained by summation of constitutive matrices $[Q(\theta_j)]$ (depending on the directions of their fibers) multiplied by their respective thicknesses t_j (Ref. 51).

A consistent load vector for distributed forces in the x and y directions is obtained by

$$\{f^m\}^T = \iint_A \lfloor N\rfloor p_{xy}\,\mathrm{d}A \tag{14}$$

Again, when the load per unit area is expressed as a function of area coordinates in polynomial form, the elements of Eq. (14) can easily be integrated analytically using the integrals in Eq. (2). The resulting consistent in-plane load vector is expressed explicitly in terms of the shape design variables x_2, x_3, and y_3.

Bending Stiffness Matrix

The displacements $U(x,y,z)$, $V(x,y,z)$, $W(x,y,z)$ at any point (x,y,z) in a midplane symmetric laminate are approximated in first-order shear deformation theory (FSDPT) using two rotation deformation functions β_x and β_y and transverse displacement w, as shown in the following equation (all functions of x and y).

$$U(x,y,z) = z\cdot\beta_x(x,y), \qquad V(x,y,z) = -z\cdot\beta_y(x,y) \tag{15}$$
$$W(x,y,z) = w(x,y)$$

The resulting bending strains can therefore be expressed in terms of the rotations β_x and β_y, as

$$\{\varepsilon^b\} = \begin{Bmatrix}\varepsilon^b_{xx}\\ \varepsilon^b_{yy}\\ \gamma^b_{xy}\end{Bmatrix} = z\begin{Bmatrix}\beta_{x,x}\\ -\beta_{y,y}\\ \beta_{x,y}-\beta_{y,x}\end{Bmatrix} = z\{\kappa\} \tag{16}$$

and the transverse shear strains are

$$\{\varepsilon^s\} = \begin{Bmatrix}\gamma_{zx}\\ \gamma_{zy}\end{Bmatrix} = \begin{Bmatrix} w,_x+\beta_x \\ w,_y-\beta_y\end{Bmatrix} \tag{17}$$

To model thin-plate behavior, in which transverse shear effects are negligible, the Kirchhoff assumption that normals to cross-sectional planes remain normal in the deformed plate must be imposed over the element:

$$w,_x+\beta_x = 0, \qquad w,_y-\beta_y = 0 \tag{18}$$

These constraints can be imposed at particular points, or in an integral manner over the element

$$\iint_A(\beta_x + w,_x)\,\mathrm{d}A = \iint_A(-\beta_y+w,_x)\,\mathrm{d}A = 0 \tag{19}$$

Assuming that each infinitesimal layer of the plate at some distance z from the reference surface is in plane stress, the bending moments are related to bending strains by

$$\{M\} = [D_b]\{\varepsilon^b\} \tag{20}$$

Now, the bending displacement and rotation fields are approximated as follows. The transverse displacement is quadratic on an element, and, consistent with the quadratic approximation of LST membrane in-plane displacements (Eqs. (4) and (5), it takes the form

$$w = \lfloor N\rfloor\{w\} \tag{21}$$

where the transverse displacements at the vertices 1–3 and midside points 4–6 are (Fig. 2)

$$\{w\}^T = [w_1 \quad w_2 \quad w_3 \quad w_4 \quad w_5 \quad w_6] \tag{22}$$

For the interpolation of normal rotations β_x and β_y, the following basis is used:

$$\beta_x = \lfloor L\rfloor\{a\} \tag{23}$$

where

$$\lfloor L\rfloor = \left\lfloor 1 \;\; \zeta_1 \;\; \zeta_2 \;\; \zeta_1^2 \;\; \zeta_1\zeta_2 \;\; \zeta_2^2 \;\; \left(2\xi_1^3+3\xi_1^2\xi_2-3\xi_1\xi_2^2-2\xi_2^3\right)\right\rfloor \tag{24}$$

and $\{a\}$ is the vector of generalized displacements. The seventh term added to the complete qudratic polynomial in Eq. (24) and an additional central node are added, as explained in Ref. 31, to make it possible to obtain the nonzero shape function values at the Loof nodes. Substituting the area coordinates of the Loof nodes and the center node makes it possible to express the generalized coordinates $\{a\}$ in terms of the rotations at the Loof nodes and center node $\{\beta_x^n\}$ (Fig. 2):

$$\left\{\beta_x^n\right\}^T = \left[\beta_{x(i)} \quad \beta_{x(ii)} \quad \beta_{x(iii)} \quad \beta_{x(iv)} \quad \beta_{x(v)} \quad \beta_{x(vi)} \quad \beta_{x(c)}\right] \tag{25}$$

leading to

$$\beta_x(\zeta_1,\zeta_2,\zeta_3) = \lfloor L(\zeta_1,\zeta_2,\zeta_3)\rfloor[A]^{-1}\left\{\beta_x^n\right\} \tag{26}$$

$$\beta_y(\zeta_1,\zeta_2,\zeta_3) = \lfloor L(\zeta_1,\zeta_2,\zeta_3)\rfloor[A]^{-1}\left\{\beta_y^n\right\} \tag{27}$$

where the matrix $[A]^{-1}$ is given explicitly in the Appendix. At each Loof node along each side of the triangle, two axes (s,n) are defined, so that the n axis is along the side (going from vertex to vertex) and an axis perpendicular to the side s. The Classical Plate Theory (CPT) Kirchoff constraints [Eq. (18)] are now imposed at the six Loof nodes i–vi,

$$\gamma_{sz} = w,_s - \beta_s = 0 \tag{28}$$

in addition to two area transverse shear constraints [Eqs. (19)]. The result is an explicit dependence of the vectors $\{\beta_x^n\}$, $\{\beta_y^n\}$ on transverse displacements at nodes 1–6 and shear rotations along the side of the triangle at the six Loof nodes:

$$\left\{\beta_x^n\right\} = [C_x]\begin{Bmatrix}\{w\}\\ \{\beta_n\}\end{Bmatrix}, \qquad \left\{\beta_y^n\right\} = [C_y]\begin{Bmatrix}\{w\}\\ \{\beta_n\}\end{Bmatrix} \tag{29}$$

where

$$\{\beta_n\}^T = \left\{\beta_{n(i)},\beta_{n(ii)},\beta_{n(iii)},\beta_{n(iv)},\beta_{n(v)},\beta_{n(vi)}\right\} \tag{30}$$

and the matrices $[C_x]$ and $[C_y]$ are given in the Appendix explicitly in terms of panel shape design variables. Substituting Eqs. (29) and (30) into Eqs. (27) and (28) yields

$$\{\beta_x\} = \lfloor L \rfloor [A^{-1}][C_x] \begin{Bmatrix} \{w^b\} \\ \{\beta_n\} \end{Bmatrix}$$
$$\{\beta_y\} = \lfloor L \rfloor [A^{-1}][C_y] \begin{Bmatrix} \{w^b\} \\ \{\beta_n\} \end{Bmatrix} \tag{31}$$

where $\lfloor L \rfloor = \lfloor L(\zeta_1, \zeta_2, \zeta_3) \rfloor$ and the matrices $[C_x]$ and $[C_y]$ depend explicitly on the shape design variables as well as on area coordinates. The transverse shear fields now depend on 12 degrees of freedom: the six transverse displacements $w_1 - w_6$ at nodes 1–6 and six rotations β_n at the six Loof nodes. From Eqs. (16) and (31) the bending strains at a distance z from the plane of symmetry can be written

$$\{\varepsilon^b\} = z \begin{Bmatrix} \lfloor L,_x \rfloor [A^{-1}][C_x] \\ -\lfloor L,_y \rfloor [A^{-1}][C_y] \\ \lfloor L,_y \rfloor [A^{-1}][C_x] - \lfloor L,_x \rfloor [A^{-1}][C_y] \end{Bmatrix} \begin{Bmatrix} \{w\} \\ \{\beta_n\} \end{Bmatrix}$$
$$= z[B^b] \begin{Bmatrix} \{w\} \\ \{\beta_n\} \end{Bmatrix} \tag{32}$$

where the $[B^b]$ matrix can be expressed explicitly in terms of area coordinates, material properties, and thickness as well as element shape design variables, using the explicit expressions

$$\lfloor L_x \rfloor = \frac{1}{J} \begin{Bmatrix} 0 \\ -y_3 \\ y \\ -2y_3\xi_1 \\ -y_3\xi_2 + y_3\xi_1 \\ 2y_3\xi_2 \\ y_3\left(6\xi_1^2 + 6\xi_1\xi_2 - 3\xi_2^2\right) + y_3\left(3\xi_1^2 - 6\xi_1\xi_2 - 6\xi_2^2\right) \end{Bmatrix} \tag{33}$$

$$\lfloor L,_x \rfloor = \frac{1}{J} \begin{Bmatrix} 0 \\ -(x_2 - X_3) \\ -x_3 \\ -2(x_2 - x_3)\xi_1 \\ -(x_2 - x_3)\xi_2 - x_3\xi_1 \\ -2x_3\xi_2 \\ -(x_2 - x_3)\left(6\xi_1^2 + 6\xi_1\xi_2 - 3\xi_2^2\right) - x_3\left(3\xi_1^2 - 6\xi_1\xi_2 - 6\xi_2^2\right) \end{Bmatrix} \tag{34}$$

If the flexural stiffness matrix for a fiber composite laminate (with layers located at distances h_k from the reference plane, see Ref. 51) is given by

$$[D_b] = \frac{1}{3} \sum_{i=1}^{n} [Q_{ij}]_k \left(h_k^3 - h_{k-1}^3\right) \tag{35}$$

then, the bending stiffness matrix for the element is

$$[K^b] = \iint_A [B^b]^T [D_b][B^b] \, \mathrm{d}A \tag{36}$$

and in order to simplify the integrand in Eq. (36), the matrix $[B^b]$ [Eq. (32)] is decomposed

$$[B^b] = [S][R] \tag{37}$$

so that

$$[S] = \begin{bmatrix} \lfloor L,_x \rfloor & 0 \\ 0 & -\lfloor L,_y \rfloor \\ \lfloor L,_y \rfloor & -\lfloor L,_x \rfloor \end{bmatrix} \tag{38}$$

$$[R] = \begin{bmatrix} [A]^{-1}[C_x] \\ [A]^{-1}[C_y] \end{bmatrix} \tag{39}$$

Because all of the components of the matrix $[R]$ are independent of the area variables, the matrix can be taken out of the integrand, leading to

$$[K_b] = (1/J)[R]^T[\bar{S}][R] \tag{40}$$

where

$$[\bar{S}] = \iint_A [S]^T [D_b][S] J \, \mathrm{d}A \tag{41}$$

Each element of the integrand in Eq. (41) is a linear combination of polynomial terms taken from Eqs. (33) and (34). Whereas the bending stiffness matrix is evaluated in Ref. 31 using seven-point numerical quadrature, here the triple product is carried out automatically using symbolic algebra,[50] and then the exact expressions for the area integrals [Eq. (2)] are used to yield a bending stiffness matrix for the element in local axes, where every element is expressed explicitly in terms of layer thickness, material properties (such as fiber angles), and shape design variables x_2, x_3, and y_3.

The consistent load vector corresponding to transverse loads is

$$\{f^b\}^T = \iint_A \lfloor N_z \rfloor p_z(\zeta_1, \zeta_2, \zeta_3) \, \mathrm{d}A \tag{42}$$

where

$$\lfloor N_z \rfloor = \lfloor \zeta_1(2\zeta_1 - 1) \quad \zeta_2(2\zeta_2 - 1) \quad \zeta_3(2\zeta_3 - 1) \quad 4\zeta_1\zeta_2 \quad 4\zeta_2\zeta_3 \quad 4\zeta_1\zeta_3 \quad 0 \quad 0 \quad 0 \quad 0 \quad 0 \quad 0 \rfloor \tag{43}$$

When a uniformly distributed load p_z is applied over the element, the load vector is

$$\{f^b\}^T = p_z \lfloor 0 \quad 0 \quad 0 \quad A/3 \quad A/3 \quad A/3 \quad 0 \quad 0 \quad 0 \quad 0 \quad 0 \quad 0 \rfloor \tag{44}$$

which through the dependence of the area A on shape design variables [Eq. (1)], is explicitly dependent on the panel's shape design variables in local coordinates.

Element Shape Design Variables and Geometric Transformation from Local to Global Coordinates

Both membrane and bending stiffness matrices are calculated in a local coordinate system in which the local x axis is aligned with the line vector from node 1 to node 2 and the z axis is perpendicular to the element plane (Fig. 1). The element stiffness matrix of the flat shell element is obtained by superposition of membrane and bending stiffness matrices. Shell membrane-bending coupling is attained through the proper spatial transformation from local to global coordinates. For an element positioned in the global axes, with vertices in global coordinates at (X_1, Y_1, Z_1), (X_2, Y_2, Z_2), and (X_3, Y_3, Z_3), a geometric transformation matrix $[T]$ between local and global coordinates is calculated using the vectors $\boldsymbol{H}$ (along side 1–2 of the triangle) and $\boldsymbol{G}$ (along side 1–3 of the triangle)

$$\{\boldsymbol{H}\} = \begin{Bmatrix} X_2 - X_1 \\ Y_2 - Y_1 \\ Z_2 - Z_1 \end{Bmatrix}, \qquad \{\boldsymbol{G}\} = \begin{Bmatrix} X_3 - X_1 \\ Y_3 - Y_1 \\ Z_3 - Z_1 \end{Bmatrix} \tag{45}$$

leading to the transformation[17]

$$[T] = \begin{bmatrix} \{\boldsymbol{l}\}^T \\ \{\boldsymbol{m}\}^T \\ \{\boldsymbol{n}\}^T \end{bmatrix} \tag{46}$$

where the local x, y, z axes are expressed by components in the global axes as vectors $\{\boldsymbol{l}\}$, $\{\boldsymbol{m}\}$, $\{\boldsymbol{n}\}$:

$$\{\boldsymbol{l}\} = \frac{\{\boldsymbol{H}\}}{|\{\boldsymbol{H}\}|}, \qquad \{\boldsymbol{n}\} = \frac{\{\boldsymbol{H}\} \times \{\boldsymbol{G}\}}{|\{\boldsymbol{H}\} \times \{\boldsymbol{G}\}|}, \qquad \{\boldsymbol{m}\} = \{\boldsymbol{n}\} \times \{\boldsymbol{l}\} \tag{47}$$

These vectors can be expressed explicitly in terms of vertex nodal coordinates in the global coordinates, for example,

$$\{\boldsymbol{l}\} = \frac{1}{\sqrt{(X_2 - X_1)^2 + (Y_2 - Y_1)^2 + (Z_2 - Z_1)^2}} \times \begin{Bmatrix} X_2 - X_1 \\ Y_2 - Y_1 \\ Z_2 - Z_1 \end{Bmatrix} \tag{48}$$

As has been discussed already and shown in Fig. 1, only three nonzero nodal coordinates exist in the local coordinate system, and these can now be expressed explicitly in terms of the nine global element shape design variables $X_1, Y_1, Z_1, X_2, Y_2, Z_2, X_3, Y_3, Z_3$:

$$\begin{aligned} x_2(X_1, Y_1, Z_1, X_2, Y_2, Z_2, X_3, Y_3, Z_3) &= \{\boldsymbol{l}\}^T\{\boldsymbol{H}\} \\ x_3(X_1, Y_1, Z_1, X_2, Y_2, Z_2, X_3, Y_3, Z_3) &= \{\boldsymbol{l}\}^T\{\boldsymbol{G}\} \\ y_3(X_1, Y_1, Z_1, X_2, Y_2, Z_2, X_3, Y_3, Z_3) &= \{\boldsymbol{m}\}^T\{\boldsymbol{G}\} \end{aligned} \tag{49}$$

It is now possible to obtain derivatives of local shape design variables x_2, x_3, y_3 with respect to nine global coordinates determining element location and orientation in the global axes. These nine coordinates $(X_1, Y_1, Z_1, X_2, Y_2, Z_2, X_3, Y_3, Z_3)$, in turn, can be expressed in terms of overall shell shape design variables defining the shape of the complete structure. This is important for the following shape sensitivity analysis, where the chain rule is used to get analytic sensitivities and where derivative calculation with respect to local coordinates can be made efficient by reducing the number of nonzero independent nodal coordinates.

The element stiffness matrix in local coordinates becomes [Eqs. (6), (7), (10), (30–32) and (36)]

$$[K^e] = \begin{bmatrix} [K^m] & 0 \\ 0 & [K^b] \end{bmatrix} \tag{50}$$

where the local degrees of freedom are in the vector $\{\bar{\boldsymbol{\delta}}^e\}$

$$\{\bar{\boldsymbol{\delta}}^e\}^T = \left\{ \{u^m\}^T \quad \{v^m\}^T \quad \{w\}^T \quad \{\beta_n\}^T \right\} \tag{51}$$

After rearranging the rows and columns of the local stiffness matrix (Eq. 50) to correspond to a reordered vector of local degrees of freedom $\{\boldsymbol{\delta}^e\}$,

$$\{\boldsymbol{\delta}^e\}^T = \left\{ u_1 \quad v_1 \quad w_1 \quad u_2 \quad , \quad , \quad w_6 \quad \beta_{n(i)} \quad , \quad \beta_{n(vi)} \right\} \tag{52}$$

The geometric transformation matrix $[T]$, which relates the local degrees of freedom to global degrees of freedom, is used to express the stiffness matrix in the global coordinates:

$$[K] = [\Lambda]^T[K^e][\Lambda] \tag{53}$$

where

$$\{\boldsymbol{\delta}^e\} = [\Lambda]\{\boldsymbol{U}\} \tag{54}$$

$$[\Lambda] = \begin{bmatrix} [T] & & & & & & & & & \\ & [T] & & & & & & & & \\ & & , & & & & & & & \\ & & & , & & & & & & \\ & & & & [T] & & & & & \\ & & & & & \pm 1 & & & & \\ & & & & & & \pm 1 & & & \\ & & & & & & & , & & \\ & & & & & & & & , & \\ & & & & & & & & & \pm 1 \end{bmatrix} \tag{55}$$

A rotational degree of freedom at a Loof node i, $\beta_{n(i)}$, on a side r–s is directed (in a vector sense) along the vector pointing from node r to node s (Fig. 2). When two neighboring triangles, triangle p and triangle q, share a side and when Loof node i on triangle p coincides with node j on triangle q, then the local directions of ${}^p\beta_{n(i)}$, ${}^q\beta_{n(j)}$ and the global directions coincide and are the same. There is, thus, no need to transform these rotational degrees of freedom from local to global coordinates. Attention must be given, however, to the directions of these rotations along a side (whether they are positive from node r to node s or from node s to node r). When both local numbering and global numbering of vertices are in ascending order along the edge, the components of transformation matrix regarding normal rotations are positive, and normal rotations have same direction.

The force vector can be written in the global coordinate using the same transformation:

$$\{\boldsymbol{f}^g\} = [\Lambda]^T\{\boldsymbol{f}^e\} \tag{56}$$

Static Analysis

Elastic displacements and rotations under load are obtained by solving the matrix equation

$$[K]\{\boldsymbol{U}\} = \{\boldsymbol{P}\} \tag{57}$$

where $[K]$ is the global stiffness matrix, $\{\boldsymbol{U}\}$ is the vector of all global degrees of freedom, and $\{\boldsymbol{P}\}$ is the global load vector. Element deformations in local coordinates are recovered from $\{\boldsymbol{U}\}$ using Eq. (54). Strains and stresses are recovered, then, using Eqs. (6–8), (32) and (35). Especially important, for the formulation of the geometric stiffness matrix are the in-plane internal loads per unit length, which, in the case of symmetric laminates are

$$\begin{Bmatrix} N_x \\ N_y \\ N_{xy} \end{Bmatrix} = [D_m]\{\varepsilon^m\} = [D_m][B^m]\begin{Bmatrix} \{u^m\} \\ \{v^m\} \end{Bmatrix} \tag{58}$$

Note that the in-plane loads are given explicitly in terms of local nodal degrees of freedom, material properties, and element local shape design variables [Eqs. (7), (9), and (11)].

Geometric Stiffness Matrix

Using the von-Karman assumptions[52] to express the nonlinear membrane strains, the well-known expressions are

$$\{\varepsilon^{\mathrm{nl}}\} = \begin{Bmatrix} \dfrac{1}{2}\,\dfrac{\partial w}{\partial x}{}^2 \\[2ex] \dfrac{1}{2}\,\dfrac{\partial w}{\partial y}{}^2 \\[2ex] \dfrac{\partial w}{\partial x}\,\dfrac{\partial w}{\partial y} \end{Bmatrix} \tag{59}$$

and the potential energy of nonlinear membrane strains can be written as

$$V = \frac{1}{2}\iint_A \begin{bmatrix} \dfrac{\partial w}{\partial x} & \dfrac{\partial w}{\partial y} \end{bmatrix} \begin{bmatrix} N_x & N_{xy} \\ N_{xy} & N_y \end{bmatrix} \begin{Bmatrix} \dfrac{\partial w}{\partial x} \\[1ex] \dfrac{\partial w}{\partial y} \end{Bmatrix} \mathrm{d}A \tag{60}$$

where $N_x(\zeta_1, \zeta_2, \zeta_3)$, $N_y(\zeta_1, \zeta_2, \zeta_3)$, $N_{xy}(\zeta_1, \zeta_2, \zeta_3)$ are in-plane internal loads per unit length obtained from the static solution. Using Eqs. (5) and (21) and rearranging rows and columns according to Eqs. (51) and (52) leads to a matrix $[G]$, which is defined as

$$\begin{Bmatrix} w_{,x} \\ w_{,y} \end{Bmatrix} \begin{Bmatrix} \lfloor \boldsymbol{N}_{,x} \rfloor \\ \lfloor \boldsymbol{N}_{,y} \rfloor \end{Bmatrix} \{w^n\} = [\bar{G}]\{\bar{\boldsymbol{\delta}}^e\} = [G]\{\bar{\boldsymbol{\delta}}^e\} \tag{61}$$

Now,

$$V = \tfrac{1}{2}\{\delta^e\}^T[K_G]\{\delta^e\} \tag{62}$$

where the element's geometric stiffness matrix is defined as

$$\left[K_G^e\right] = \iint_A [G]^T \begin{bmatrix} N_x & N_{xy} \\ N_{xy} & N_y \end{bmatrix} [G]\,\mathrm{d}A \tag{63}$$

and transformation from local to global coordinates leads to

$$[K_G] = [A]^T\left[K_G^e\right][A] \tag{64}$$

Because the membrane forces are expressed in closed form in terms of nodal displacements and material properties [Eq. (58)], those can be directly substituted into Eq. (63) for the explicit formulation of geometric stiffness matrix. But this is not desirable when considering effective derivation of the shape sensitivities because all of the nodal displacements of the element [Eq. (58)] will be included in the geometric stiffness matrix, and, thus, a corresponding number of derivative matrices will be needed in chain rule differentiation, using the shape sensitivities of the static solution [Eq. (57)].

For the effective calculation of geometric stiffness sensitivity, the number of physical variables needs to be reduced. The LST membrane element produces linear stresses in the area coordinates when midside nodes are used, and, then, stresses at any three points can reproduce the stress distribution in the element. To get the explicit formulation of geometric stiffness, the following interpolation is used for the stress distribution:

$$N_x = \lfloor 1 \quad \xi_1 \quad \xi_2 \rfloor \begin{Bmatrix} b_1 \\ b_2 \\ b_3 \end{Bmatrix} \tag{65}$$

Using Eq. (58), membrane forces are calculated at three Gaussian points, and applying Eq. (65) at these points leads to expressions for in-plane loads in terms of their values at these three points.

$$N_x = \lfloor 1 \quad \xi_1 \quad \xi_2 \rfloor [B]^{-1} \begin{Bmatrix} N_{x1} \\ N_{x2} \\ N_{x3} \end{Bmatrix} \tag{66}$$

Similarly, N_y and N_{xy} can be expressed in terms of resultant forces at Gaussian points and of area coordinates. By substituting Eq. (66) into Eq. (63), only nine components of the membrane forces are required for the interpolation of membrane forces over the element.

Now all of the matrices in Eq. (63) are explicit in terms of area coordinates, nine values of in-plane loads N_{ij} at three Gaussian points, local shape design variables in the form of local coordinates of vertices, and material properties. When the triple product of the integrand in Eq. (63) is carried out using automated symbolic algebra,[50] the result (for each element of the element's geometric stiffness matrix) is a linear combination of polynomials in area coordinates. Using the explicit expressions for these integrals, the element's stiffness matrix is found explicitly. It can then be transformed to global coordinates

$$[K_G] = (1/J)[\Lambda]^T[\bar{K}_G][\Lambda] \tag{67}$$

where

$$[\bar{K}_G] = \iint_A [G]^T \begin{bmatrix} N_x & N_{xy} \\ N_{xy} & N_y \end{bmatrix} [G] J\,\mathrm{d}A \tag{68}$$

Bifurcation Buckling Analysis

In linear buckling analysis of a structure, the system equations are expressed in the form

$$[[K] + \lambda_i[K_G]]\{\phi_i\} = \{0\} \tag{69}$$

where $[K]$ and $[K_G]$ are stiffness and geometric stiffness matrices of order n, λ_i, and $\{\phi_i\}$ are eigenvalue and corresponding eigenvector. The eigenvalue λ determines by how much the loads on the structure have to be increased or decreased to obtain an equilibrium bifurcation point. For a structure to be buckling safe, all eigenvalues must be larger than one. A typical buckling constraint is written as

$$g = 1 - \lambda_{\min} \leq 0 \tag{70}$$

Large-scale symmetric eigenvalue problems of the type shown in Eq. (69) are solved routinely today in the context of structural analysis, in buckling and also in structural dynamics, where vibration mode shape and natural frequencies are calculated using the stiffness and mass matrices of a structure. There is an important difference between the structural dynamic modeling needs in airframe design and the buckling-analysis needs. Overall airframe static and dynamic aeroelastic responses involve global deformation of the structure (such as wing bending or torsion) while local vibrations (such as panel vibrations or spar web vibrations) are less important in transonic airplane design, and, thus, airplane aeroelastic mathematical models need not be of very high order. A design-oriented modeling approach for buckling, however, as pursued here, where with one structural model both global and local buckling failure modes (or buckling caused by subcomponent interactions) can be captured, makes it necessary to use fine finite element meshes and many degrees of freedom. The resulting large-scale eigenvalue problems are solved, in the capability described in this article, using a Lanczos algorithm for generalized symmetric eigenvalue problems.[53]

Analytic Sensitivities

A significant amount of experience already exists in the area of sensitivity analysis of finite element structural behavior, covering problems involving static and dynamic deformation and stress as well as vibration and buckling.[54,55] Because of the complexity of shell finite elements, the sensitivity analysis of these elements in general (especially in the case of shape design variables) is quite challenging, and in most practical cases shape sensitivities had been obtained using finite difference or semianalytic differentiation, even though the numerical problems associated with these techniques are well known.[54] Automatic differentiation[56] can be applied, of course, to existing computer subroutines already used for the generation of shell element stiffness and geometric stiffness matrices. However, because most shell element matrices rely on numerical quadrature for area integration, they are computationally expensive. Modifying existing codes to include sensitivities using automatic differentiation will lead to expensive sensitivity computation as well. When numerical quadrature is used, even using analytic derivation of element sensitivities[57,58] will still lead to considerable computational cost of evaluating both the element matrices and their sensitivities because in this case the sensitivity with respect to nodal positions must be obtained at each Gaussian point.

In the preceding sections explicit mathematical expressions in terms of thickness (sizing), material, and shape design variables were given for all steps required in the static analysis and corresponding linear buckling analysis of thin-walled structures. Extending the usage of automated symbolic equation derivation to obtain explicit expressions for the derivatives follows naturally. The capability of Ref. 50 was used to obtain sensitivities of element matrices in the local coordinate system. These were, then, combined with sensitivities of element vertices in the global coordinates with respect to shape design variables used to parameterize the overall shape of the structure.

Let q_i be a global shape design variable. First the derivatives of node locations in the global coordinates, $\partial\Psi_j/\partial q_i$ are calculated. Using the derivative of the geometric transformation matrix [which can be done by calculating the derivative of individual components, Eqs. (46) and (55)] the derivative of the element's contribution to the global stiffness matrix can be written as

$$\frac{\partial[K]}{\partial q_i} = \frac{\partial[\Lambda]^T}{\partial q_i}[K^e][\Lambda] + [\Lambda]^T\frac{\partial[K^e]}{\partial q_i}[\Lambda] + [\Lambda]^T[K^e]\frac{\partial[\Lambda]}{\partial q_i} \tag{71}$$

and the derivative of nodal locations in the local coordinates (ψ_k) are calculated using chain rule

$$\frac{\partial \psi_k}{\partial q_i} = \frac{\partial \psi_k}{\partial \Psi_j}\frac{\partial \Psi_k}{\partial q_i} \tag{72}$$

Because the components of the element stiffness matrix are explicit functions of the location of nodes in local coordinates, the derivative of the element stiffness matrix becomes

$$\frac{\partial [K^e]}{\partial q_i} = \frac{\partial [K^e]}{\partial \psi_k}\frac{\partial \psi_k}{\partial q_i} \tag{73}$$

The explicit element stiffness matrix representing bending [Eq. (40)] is

$$[K^b] = (1/J)[R]^T[\bar{S}][R] \tag{74}$$

where both $[R]$ and $[\bar{S}]$ contain nodal coordinates and where material properties are included in $[\bar{S}]$. Element bending stiffnesses for orthotropic material depend on the direction of the local coordinate system, which is calculated from nodal locations in the global coordinates. The derivatives of material properties must, thus, be included (they are zero for isotropic materials). As a result, the derivative of element bending stiffness matrix is

$$\frac{\partial [K^b]}{\partial q_i} = \frac{\partial [K^b]}{\partial \psi_k}\frac{\partial \psi_k}{\partial q_i} + \frac{\partial [K^b]}{\partial \Psi_j}\frac{\partial \Psi_j}{\partial q_i} \tag{75}$$

where

$$\frac{\partial [K^b]}{\partial \psi_k} = \frac{\partial (1/J)}{\partial \psi_k}[R]^T[\bar{S}][R] + \frac{1}{J}\quad\frac{\partial [R]^T}{\partial \psi_k}[\bar{S}][R]$$

$$+ [R]^T\frac{\partial [\bar{S}]}{\partial \psi_k}[R] + [R]^T[\bar{S}]\frac{\partial [R]}{\partial \psi_k} \tag{76}$$

$$\frac{\partial [K^b]}{\partial \Psi_j} = \frac{1}{j}[R]^T\frac{\partial [\bar{S}]}{\partial \Psi_j}[R]$$

Similarly, for the membrane stiffness matrix [Eqs. (12) and (13)]

$$\frac{\partial [K^m]}{\partial q_i} = \frac{\partial [K^m]}{\partial \psi_k}\frac{\partial \psi_k}{\partial q_i} + \frac{\partial [K^m]}{\partial \Psi_j}\frac{\partial \Psi_j}{\partial q_i} \tag{77}$$

where

$$\frac{\partial [K^m]}{\partial \psi_k} = \frac{\partial (1/J)}{\partial \psi_k}[\bar{K}^m] + \frac{1}{J}\frac{\partial [\bar{K}^m]}{\partial \psi_k} \tag{78}$$

$$\frac{\partial [\bar{K}^m]}{\partial \Psi_j} = \frac{1}{J}\frac{\partial [\bar{K}^m]}{\partial \Psi_j} \tag{79}$$

Using explicit expressions for the consistent load vectors [Eqs. (14), (42–44), and (56)], shape sensitivity of the force vector is easily obtained. It is now possible to obtain the derivative of the static solution [Eq. (57)] analytically using the already decomposed global stiffness matrix[54]:

$$[K]\left\{\frac{\partial U}{\partial q}\right\} = \left\{\frac{\partial P}{\partial q}\right\} - \left[\frac{\partial [K]}{\partial q}\right]\{\boldsymbol{U}\} \tag{80}$$

By taking derivatives of Eqs. (67) and (68), the following sensitivities of geometric stiffness are now obtained:

$$\frac{\partial [K_G]}{\partial q_i} = \frac{\partial (1/J)}{\partial q_i}[\Lambda]^T[\bar{K}_G[\Lambda] + \frac{1}{J}\quad\frac{\partial [\Lambda]^T}{\partial q_i}[\bar{K}_G][\Lambda]$$

$$+ [\Lambda]^T\frac{\partial [\bar{K}_G]}{\partial q_i}[\Lambda] + [\Lambda]^T[\bar{K}_G]\frac{\partial [\Lambda]}{\partial q_i} \tag{81}$$

and because the matrix $[\bar{K}_G]$ is a function of membrane forces at three Gaussian points as well as of nodal coordinates, its sensitivity can be obtained by

$$\frac{\partial [\bar{K}_G]}{\partial q_i} = \frac{\partial [\bar{K}_G]}{\partial \psi_k}\frac{\partial \psi_k}{\partial q_i} + \frac{\partial [\bar{K}_G]}{\partial \{N_{\rm mk}\}}\frac{\partial \{N_{\rm mk}\}}{\partial q_i} \tag{82}$$

Using the explicit equations for in-plane internal forces in terms of the deformation vector $\{\boldsymbol{U}\}$ and element sizing, material, and geometry [Eqs. (58) and (66)], the derivatives of N_x, N_y, and N_{xy} evaluated at the three Gaussian points of the triangle are obtained explicitly in closed form using symbolic derivation. With

$$\{N_m\} = [D_m][B_m][T_m]\{\boldsymbol{U}\} \tag{83}$$

sensitivities of the membrane forces are calculated at the three Gaussian points as

$$\frac{\partial \{N_{\rm mk}\}}{\partial q_i} = \frac{\partial [D_m]}{\partial q_i}[B_m][T_m]\{\boldsymbol{U}\} + [D_m]\frac{\partial [B_m]}{\partial q_i}[T_m]\{\boldsymbol{U}\}$$

$$+ [D_m][B_m]\frac{\partial [T_m]}{\partial q_i}\{U\} + [D_m][B_m][T_m]\frac{\partial \{\boldsymbol{U}\}}{\partial q_i} \tag{84}$$

Sensitivity of Buckling Load and Buckling mode Shapes

Now that the sensitivities of the $[K]$ and $[K_G]$ matrices ($\partial [K]/\partial q_i$ and $\partial [K_G]/\partial q_i$) are available analytically, the sensitivity of buckling eigenvalues (in the case of distinct eigenvalues) and, hence, the sensitivity of buckling constraints is given by[54,55]

$$\frac{\partial g}{\partial q_i} = -\frac{\partial \lambda}{\partial q_i} = \frac{\{\phi\}^T[\partial [K]/\partial q_i + \lambda(\partial [K_G]/\partial q_i)]\{\phi\}}{\{\phi\}^T[K_G]\{\phi\}} \tag{85}$$

Also the sensitivity of eigenvector with respect to the design variable is obtained from[59]

$$[B_i]\left\{\frac{\partial \phi_i}{\partial q_i}\right\} = \{F_i\} \tag{86}$$

where

$$[B_i] = ([K] + \lambda_i[K_G]) \tag{87}$$

$$\{F_i\} = -\quad\frac{\partial [K]}{\partial q_i} + \lambda_i\frac{\partial [K_G]}{\partial q_i} + \frac{\partial \lambda_i}{\partial q_i}[K_G]\quad\{\phi_i\} \tag{88}$$

Test Cases and Numerical Results

A thorough assessment of the accuracy of analysis results and corresponding analytic sensitivity results obtained with the present capability can be found in Ref. 60 for a variety of test cases including rectangular, skew, and triangular isotropic and composite panels, as well as thin-walled channels and a representative fighter wing structure. The test cases and results described here are selected to demonstrate buckling analysis/sensitivity of realistic three-dimensional structures made of assemblies of curved and flat plates. The thin-walled rectangular channel is chosen because of the availability of theoretical results and its variety of modes of buckling depending on its shape. The model fighter wing is similar in geometry to an actual lightweight fighter wing, with a somewhat simplified layout of its internal structure. The size and complexity of the fighter wing model are representative of wing structural models used in preliminary design. As results will show, under high load factor pull-up loads buckling failure modes switch as the planform of the wing changes shape, and neighboring panels and corresponding spar/rib webs buckle together.

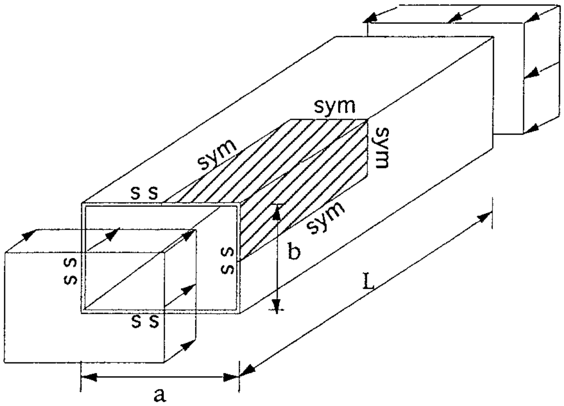

Fig. 3 Geometry of the slender thin-walled channel section.

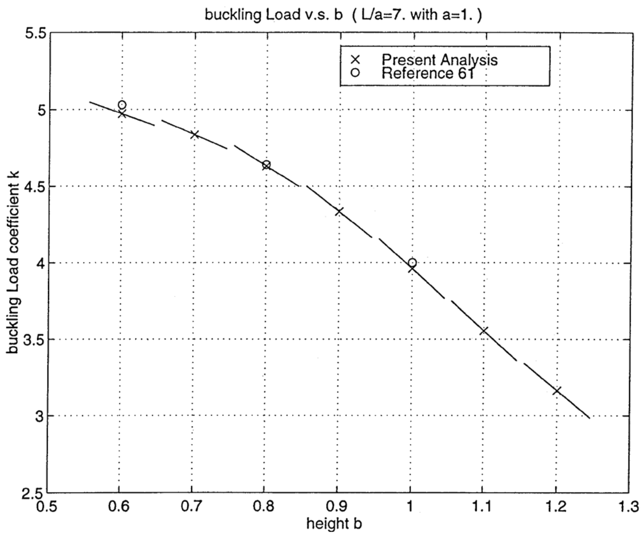

Fig. 4 Variation of buckling eigenvalues and analytic shape sensitivities for the slender channel as a function of cross-sectional shape *b/a*.

Figure 3 shows a thin-walled long channel section subject to compressive loads for which analytical buckling results, including results for buckling modes involving interactions between neighboring plate segments, are available.[61] The length of the channel is L, and its cross sectional width and height are a and b, respectively. Wall thickness is constant, and the material is isotropic. The channel is simply supported at its open ends in the planes of the cross sections, and it is subject to a uniaxial compressive force per unit length N in the direction of its axis. Theoretical results[61] are available for this case when the lenth of the channel is large relative to its cross-sectional dimensions. In the test cases examined here the L/a ratio is 7.0, and the wall-thickness to cross-sectional width ratio $t/a = \frac{1}{100}$. Because the structure and the applied loads are symmetric, only one-eighth of the channel is analyzed. The flat-plate walls of the channel are assumed to be connected rigidly, so that the undeformed right angles between upper panels and side panels remain right angles as the structure deforms.

For shape sensitivity analysis the height of the channel b is chosen as a shape design variable. The numerical results for both buckling and buckling sensitivity analysis are shown in Fig. 4, covering design variable changes from $b = 0.6$ to 1.2 (with $a = 1.0$). A buckling mode shape for a given geometry $b/a = 1.0$ is shown in Fig. 5. The buckling load coefficient shown in Fig. 4 is defined by the equation for the critical buckling load:

$$N_{\mathrm{cr}} = \frac{K\pi^2 Et}{12(1-\nu^2)a^2} \tag{89}$$

As can be seen, accuracies of the finite element (FE) analysis and analytic sensitivities using the new capability are excellent.

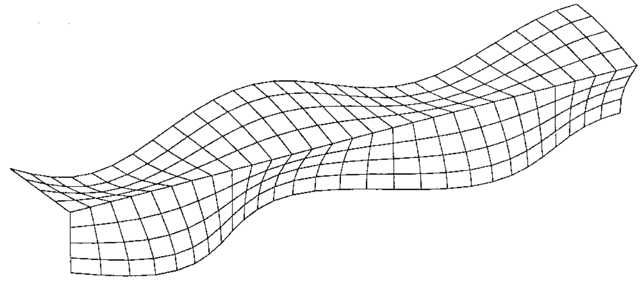

Fig. 5 Typical critical buckling mode shape for the channel, *b/a* = 1.

Figures 6 and 7 show the two lowest buckling mode shapes on an all aluminum representative lightweight fighter wing in a $9g$ pull-up maneuver. The wing box is subject to distributed loads over its upper skin. It has an array of 11 (including leading edge and trailing edge) spars and 4 ribs, typical of what is used in fighter wing design to create multiple load paths, reduce the size of skin panels (and thus reduce skin weight needed to stabilize skin panels against buckling), and also provide hard points for external store pylons, as well as for leading-edge and trailing-edge high lift devices. The wing has a 3.5% thick parabolic airfoil. The FE model consists of 354 flat shell elements for ribs and spars as well as wing skins, a somewhat coarse mesh because the emphasis in the cases reported here is to validate the accuracy of the analytic shape sensitivity analysis and finer meshes would lead to very large FE problems requiring considerable computational resources. The total number of degrees of freedom, after application of cantilever boundary conditions at the root, is 2457.

As can be seen, in both buckling mode shapes shown the buckling involves neighboring panels and the supporting structure around them. The current model captures this local failure and overall wing deformation and stresses accurately as well. When planform shape variations are introduced, the leading-edge sweep angle serves as a shape design variable, and the wing is allowed to change shape (Fig. 8) while keeping loads on the nodes of the upper skin constant. Figure 9 shows the variation of the two lowest buckling roots as the wing shape (leading-edge sweep angle) is varied. Analytic shape sensitivities calculated at each point (shown as short straight lines at each point) are excellent, even though the parametric results themselves are noisy and non-smooth.

If only analysis results are sought, this numerical noise in Fig. 9 is of small magnitude, and accuracy of the analysis at each leading-edge sweep angle is good. However, if this analysis capability is used to obtain sensitivities via finite difference or semianalytic techniques, considerable errors in sensitivity predictions can be expected. These problems with finite difference or semianalytic differentiation when certain disciplinary analysis codes portray non-smooth behavior in the context of multidisciplinary design optimization (MDO) are well known.[62] In our case the nonsmoothness was traced and found to originate, not surprisingly, in the stress recovery at the element's Gaussian points (to be, then, used to evaluate the geometric stiffness matrix). The analytic sensitivites, as Fig. 9 shows, are always accurate and reliable.

If we name the nine upper skin panels between the first and second ribs sp1, sp2, ... sp9 (starting near the trailing edge and moving toward the leading edge), we notice that upper skin panel sp1 and adjacent panel sp2 buckle in the Mode A, while Mode B is characterized by the buckling of three connected panels from sp5 to sp7. In both cases there are interactions with the neighboring support structure.

It is interesting to compare buckling load coefficients obtained from global buckling analysis to those obtained in the conventional way using individual panels with simply supported boundaries. The local buckling analysis is attempted for isolated panels based on stresses obtained from stress analysis of the whole structure. Two upper skin panels located between the first and second ribs are chosen for the local analysis, and each panel is assumed to buckle independently from the other panels. The first one (sp1) is the skin panel

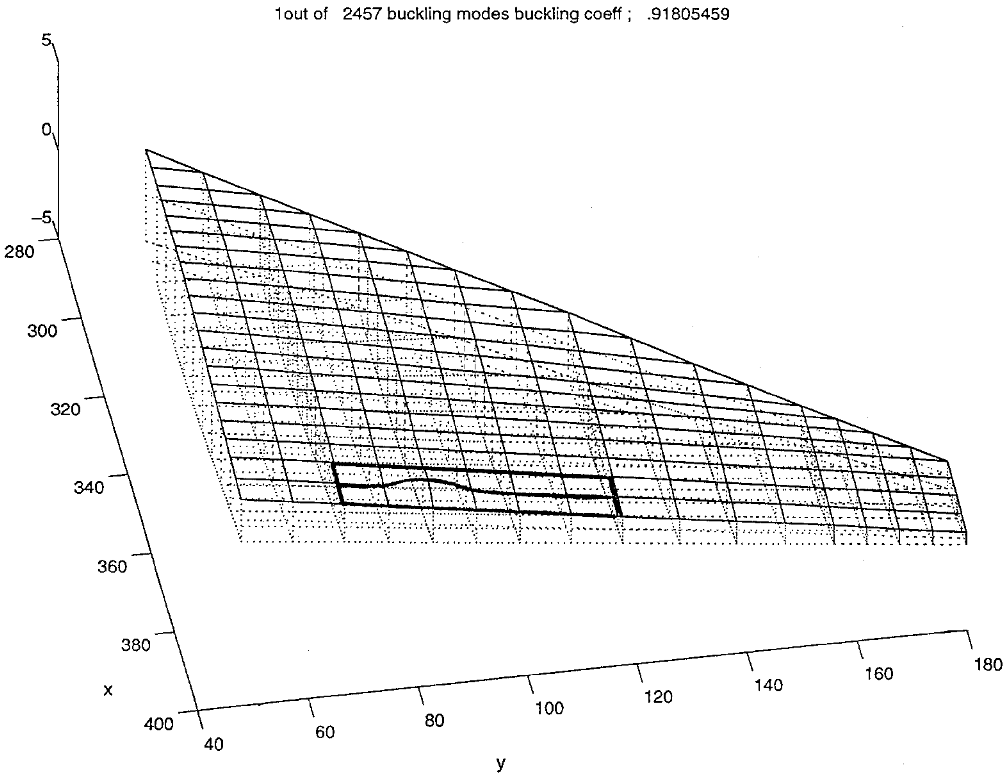

Fig. 6 First buckling mode shape for the wing; leading-edge sweep angle = 35.125.

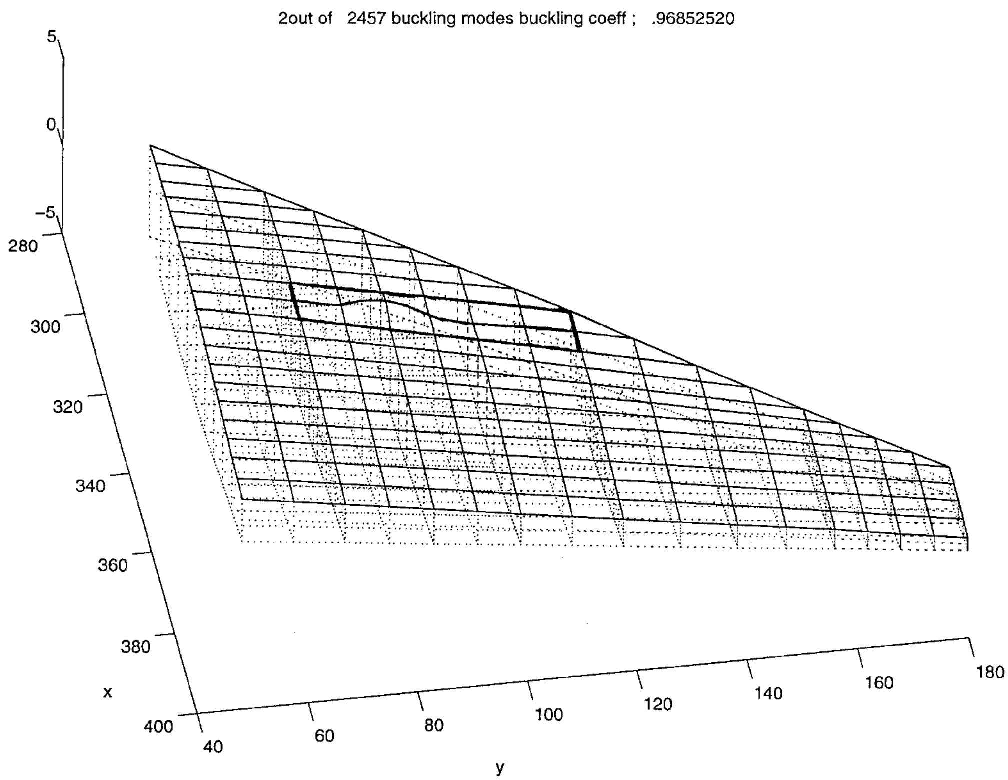

Fig. 7 Second buckling mode shape for the wing, leading-edge sweep angle = 35.125.

attached to the trailing-edge spar. The other one (sp6) is located between the sixth spar and seventh spar from the trailing-edge. The buckling of these two panels seems to be dominant in the first and second modes of the global buckling analysis as shown in Figs. 6 and 7. The same finite element mesh as in global finite element model is used to obtain the buckling load coefficients of the isolated panels. As expected, the critical λ for the isolated skin panel sp1 is 0.879 while the corresponding λ for buckling global mode shape A is 0.918. The critical λ for the isolated skin panel sp6 is 0.95, whereas the corresponding λ for buckling global mode shape A is 0.968. This is consistent with the results of Ref. 12 because interaction of neighboring panels and spar or rib webs tends, in many cases, to stiffen a panel compared with the simply supported boundary conditions used usually in individual panel analysis.

Note, as Fig. 9 shows, that a single FE model captures all buckling modes, whether local or global. Switching of modes, when panels

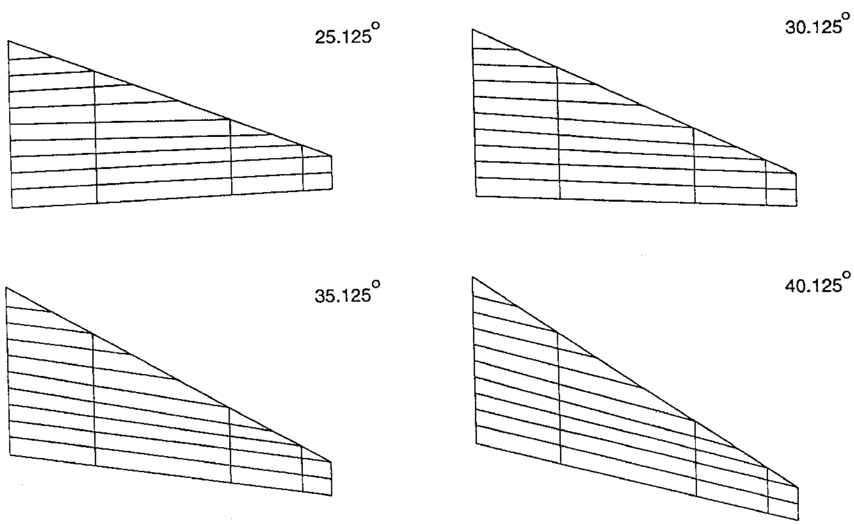

Fig. 8 Four wing planforms, corresponding to variation of leading-edge sweep.

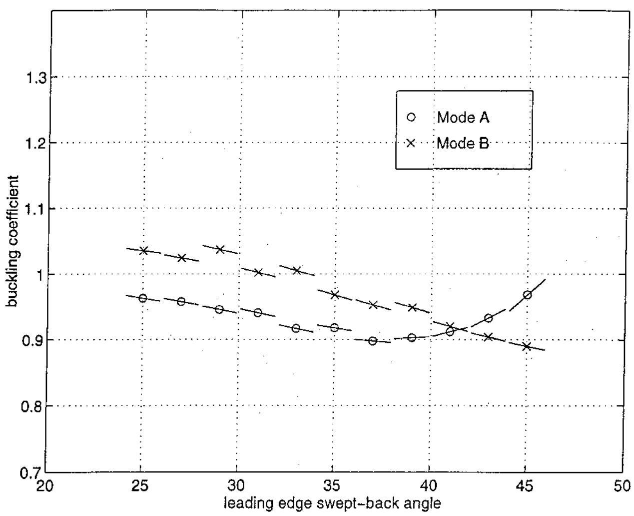

Fig. 9 Variation of bucking eigenvalues and analytic shape sensitivities for the fighter wing box as a function of leading-edge sweep angle.

or panel combinations become less critical or more critical when the shape is evolving during design, presents no problem, whereas when panels are analyzed for buckling individually there is always a danger that a critical panel will be missed.

Conclusions

The mathematical formulation of the flat triangular DKT/LST shell element with Loof nodes was modified and adapted in order to obtain explicit closed-form expressions for element stiffness and geometric stiffness matrices in terms of sizing, material, and shape design variables. Automated symbolic equation derivation and closed-form expressions for area integrals were used in the process. The resulting equations were used to derive explicit expressions for the analytic sensitivities of stiffness and geometric stiffness matrices with respect to shell sizing, material, and shape design variables. With analytic shape sensitivities of structural matrices and corresponding buckling eigenvalues at hand, the resulting new computer capability makes it possible to construct buckling constraint approximations for approximation-concepts-based structural synthesis. The simplicity of the shell elements used and the elimination of the need to carry out numerical integration lead to computational savings, especially when repetitive analyses have to be carried out during shape design optimization of typical airframes. The new capability can capture both local and global modes of buckling failure with the same FE model. Subcomponent interaction during buckling can, thus, be taken into account during shape optimization of wing and fuselage structures.

In the results presented in this paper and in the work supporting it, accuracy of the bucking predictions as well as accuracy of the analytic sensitivities were demonstrated. Low-level numerical noise, leading to nonsmooth buckling predictions when shape design variables were varied, was detected and found to be caused by nonsmoothness of element in-plane stresses. Whereas the stiffness matrix and deformation static solutions were found to be smooth, the nonsmooth stresses led to a nonsmooth geometric stiffness matrix and, hence, to nonsmooth buckling eigenvalues. At the same time the analytic shape sensitivities were found to be always accurate, leading to an efficient and reliable design-oriented structural modeling capability.

Appendix: Explicit Expressions for the A and C Matrices (Ref. 31)

$$[A]^{-1} = \begin{matrix} 0.3333333 & 0.3333333 & -0.2440168 & 0.9106835 & 0.9106838 & -0.2440169 & -1 \\ -1.422650 & -2.577348 & 2.041450 & -6.041449 & 1.577348 & 0.4226499 & 6.0 \\ -2.577349 & -1.422650 & 0.4226499 & 1.577350 & -6.041451 & 2.041451 & 6.0 \\ -1.464101 & 5.464098 & -4.928200 & 8.928199 & -6.196150 & 4.196151 & -6.0 \\ 5.0 & 5.0 & -4.464100 & 2.464100 & 2.464100 & -4.464100 & -6.0 \\ 5.464099 & -1.464100 & 4.196151 & -6.196150 & 8.928201 & -4.928201 & -6.0 \\ 1.732051 & -1.732050 & 1.732051 & -1.732051 & 1.732051 & -1.732051 & 0.0 \end{matrix} \tag{A1}$$

$$
[Cx] = \begin{bmatrix}
-c_1\frac{x_{12}}{l_{12}^2} & -c_2\frac{x_{12}}{l_{12}^2} & 0 & c_3\frac{x_{12}}{l_{12}^2} & 0 & 0 & -\frac{y_{12}}{l_{12}} & 0 & 0 & 0 & 0 & 0 \\
c_2\frac{x_{12}}{l_{12}^2} & c_1\frac{x_{12}}{l_{12}^2} & 0 & -c_3\frac{x_{12}}{l_{12}^2} & 0 & 0 & 0 & -\frac{y_{12}}{l_{12}} & 0 & 0 & 0 & 0 \\
0 & -c_1\frac{x_{23}}{l_{23}^2} & -c_2\frac{x_{23}}{l_{23}^2} & 0 & c_3\frac{x_{23}}{l_{23}^2} & 0 & 0 & 0 & -\frac{y_{23}}{l_{23}} & 0 & 0 & 0 \\
0 & c_2\frac{x_{23}}{l_{23}^2} & c_1\frac{x_{23}}{l_{23}^2} & 0 & -c_3\frac{x_{23}}{l_{23}^2} & 0 & 0 & 0 & 0 & -\frac{y_{23}}{l_{23}} & 0 & 0 \\
c_2\frac{x_{13}}{l_{13}^2} & 0 & c_1\frac{x_{13}}{l_{13}^2} & 0 & 0 & -c_3\frac{x_{13}}{l_{13}^2} & 0 & 0 & 0 & 0 & \frac{y_{13}}{l_{13}} & 0 \\
-c_1\frac{x_{13}}{l_{13}^2} & 0 & -c_2\frac{x_{13}}{l_{13}^2} & 0 & 0 & c_3\frac{x_{13}}{l_{13}^2} & 0 & 0 & 0 & 0 & 0 & \frac{y_{13}}{l_{13}} \\
\alpha_1 & \alpha_2 & \alpha_3 & c_4\frac{y_{13}}{A} & c_4\frac{y_{23}}{A} & -c_4\frac{y_{13}}{A} & c_5\frac{y_{12}}{l_{12}} & c_5\frac{y_{12}}{l_{12}} & c_5\frac{y_{23}}{l_{23}} & c_5\frac{y_{23}}{l_{23}} & -c_5\frac{y_{13}}{l_{13}} & -c_5\frac{y_{13}}{l_{13}}
\end{bmatrix} \tag{A2}
$$

$$
[Cy] = \begin{bmatrix}
c_1\frac{y_{12}}{l_{12}^2} & c_2\frac{y_{12}}{l_{12}^2} & 0 & -c_3\frac{y_{12}}{l_{12}^2} & 0 & 0 & -\frac{x_{12}}{l_{12}} & 0 & 0 & 0 & 0 & 0 \\
-c_2\frac{y_{12}}{l_{12}^2} & -c_1\frac{y_{12}}{l_{12}^2} & 0 & c_3\frac{y_{12}}{l_{12}^2} & 0 & 0 & 0 & -\frac{x_{12}}{l_{12}} & 0 & 0 & 0 & 0 \\
0 & c_1\frac{y_{23}}{l_{23}^2} & c_2\frac{y_{23}}{l_{23}^2} & 0 & -c_3\frac{y_{23}}{l_{23}^2} & 0 & 0 & 0 & -\frac{x_{23}}{l_{23}} & 0 & 0 & 0 \\
0 & -c_2\frac{y_{23}}{l_{23}^2} & -c_1\frac{y_{23}}{l_{23}^2} & 0 & c_3\frac{y_{23}}{l_{23}^2} & 0 & 0 & 0 & 0 & -\frac{x_{23}}{l_{23}} & 0 & 0 \\
-c_2\frac{y_{13}}{l_{13}^2} & 0 & -c_1\frac{y_{13}}{l_{13}^2} & 0 & 0 & c_3\frac{y_{13}}{l_{13}^2} & 0 & 0 & 0 & 0 & \frac{x_{13}}{l_{13}} & 0 \\
c_1\frac{y_{13}}{l_{13}^2} & 0 & c_2\frac{y_{13}}{l_{13}^2} & 0 & 0 & -c_3\frac{y_{13}}{l_{13}^2} & 0 & 0 & 0 & 0 & 0 & \frac{x_{13}}{l_{13}} \\
\alpha_4 & \alpha_5 & \alpha_6 & c_4\frac{x_{12}}{A} & c_4\frac{x_{23}}{A} & -c_4\frac{x_{13}}{A} & c_5\frac{x_{12}}{l_{12}} & c_5\frac{x_{12}}{l_{12}} & c_5\frac{x_{23}}{l_{23}} & c_5\frac{x_{23}}{l_{23}} & -c_5\frac{x_{13}}{l_{13}} & -c_5\frac{x_{13}}{l_{13}}
\end{bmatrix} \tag{A3}
$$

where

$$
x_{ij} = x_i - x_j, \qquad y_{ij} = y_i - y_j, \qquad l_{ij} = \sqrt{x_{ij}^2 + y_{ij}^2} \tag{A4}
$$

$$
c_1 = 2.1547004, \qquad c_2 = 0.1547004, \qquad c_3 = 2.3094008, \qquad c_4 = 1.3333334, \qquad c_5 = 0.16666667 \tag{A5}
$$

and

$$
\begin{aligned}
\alpha_1 &= 0.3333328 \left(\frac{x_{12}}{l_{12}^2} + \frac{x_{13}}{l_{13}^2} - \frac{y_{23}}{A}\right), & \alpha_2 &= 0.3333328 \left(-\frac{x_{12}}{l_{12}^2} + \frac{x_{23}}{l_{23}^2} + \frac{y_{13}}{A}\right) \\
\alpha_3 &= -0.3333328 \left(\frac{x_{23}}{l_{23}^2} + \frac{x_{13}}{l_{13}^2} + \frac{y_{12}}{A}\right), & \alpha_4 &= -0.3333328 \left(\frac{y_{12}}{l_{12}^2} + \frac{y_{13}}{l_{13}^2} + \frac{x_{23}}{A}\right) \\
\alpha_5 &= 0.3333328 \left(\frac{y_{12}}{l_{12}^2} - \frac{y_{23}}{l_{23}^2} + \frac{x_{13}}{A}\right), & \alpha_6 &= 0.3333328 \left(\frac{y_{23}}{l_{23}^2} + \frac{y_{13}}{l_{13}^2} - \frac{x_{12}}{A}\right)
\end{aligned} \tag{A6}
$$

Acknowledgments

Support from the National Science Foundation and the NASA Ames Research Center is greatly appreciated. The authors would also like to thank Keith Holsapple from the Department of Aeronautics and Astronautics at the University of Washington for his help and support.

References

[1]Haftka, R. T., and Gurdal, Z., *Elements of Structural Optimization*, 3rd ed., Kluwer Academic, Norwell, MA, 1991, Chap. 11.

[2]Schmit, L. A., and Ramanathan, R. K., "Multilevel Approach to Minimum Weight Design Including Buckling Constraints," *AIAA Journal*, Vol. 16, No. 2, 1978, pp. 97–104.

[3]Starnes, J. H., Jr., and Haftka, R. T., "Preliminary Design of Composite Wings for Buckling, Stress and Displacement Constraints," *Journal of Aircraft*, Vol. 16, No. 8, 1979, pp. 564–570.

[4]Schmit, L. A., and Mehrinfar, M., "Multilevel Optimum Design of Structures with Fiber-Composite Stiffened-Panel Components," *AIAA Journal*, Vol. 20, No. 1, 1982, pp. 138–147.

[5]McCullers, L. A., "Automated Design of Advanced Composite Structures," *Mechanics of Composite Materials*, edited by Zvi Hashin, Pergamon, New York, 1983, pp. 119–133.

[6]Hornung, G., Mathias, D. W., and Rohle, H., "Optimization of Wing Type Structures Including Stress and Buckling Constraints," Third Air Force/NASA Symposium on Recent Advances in Multidisciplinary Analysis and Optimization, San Francisco, Sept. 1990.

[7]Lecina, G., and Petiau, C., "Advances in Optimal Design with Composite Materials," *Computer Aided Optimal Design: Structural and Mechanical Systems*, edited by C. A. Mota Soares, Springer–Verlag, Berlin, 1987, pp. 943–953.

[8]Ausman, J. D., Hangen, J. A., and Acevedo, D. A., "Application of a Local Panel Buckling Constraint Within Automated Multidisciplinary Structural Analysis and Design," AIAA Paper 92-1116, Feb. 1992.

[9]Bartholomew, P., Harris, J., and Wellen, H., "The Integration of Local Design of Composite Panels into Overall Structural Design," AIAA Paper 94-4354, 1994.

[10]Eschenauer, H. A., Schuhmacher, G., and Hartzheim, W., "Multidisciplinary Design of Composite Aircraft Structures by Lagrange," *Computers and Structures*, Vol. 44, No. 4, 1992, pp. 877–893.

[11]Ragon, S. A., Gurdal, Z., and Starnes, J. H., Jr., "Optimization of Composite Box-Beam Structures Including the Effects of Subcomponent Interaction," AIAA Paper 94-1410, April 1994.

[12]Ragon, S. A., and Gurdal, Z., "Effects of Geometric Nonlinearities on the Response of Optimized Box Beam Structures," AIAA Paper 93-1412, April 1993.

[13]Haftka, R. T., and Gurdal, Z., *Elements of Structural Optimization*, 3rd ed., Kluwer Academic, Norwell, MA, 1991, Chap. 7.

[14]Livne, E., "Analytic Sensitivities for Shape Optimization in Equivalent Plate Structural Wing Model," *Journal of Aircraft*, Vol. 31, No. 4, 1994, pp. 961–969.

[15]Harvey, M. S., "Automated Finite Element Modeling of Wing Structures for Shape Optimization," M.Sc. Thesis, Dept. of Aeronautics and Astronautics, Univ. of Washington, Seattle, WA, 1993.

[16]Singhvi, S., and Kapania, R. K., "Analytical Shape Sensitivities and Approximations of Modal Response of Generally Laminated Tapered Skew Plates," AIAA Paper 92-2391, April 1992.

[17]Langelaan, J. W., and Livne, E., "Analytic Sensitivities and Design Oriented Structural Analysis for Airplane Fuselage Shape Synthesis," *Computers and Structures*, Vol. 62, No. 3, 1997, pp. 505–519.

[18]Batkin, M. E., "Shape Optimization of Plate and Shell Structures," *AIAA Journal*, Vol. 20, No. 2, 1982, pp. 268–273.

[19]Haftka, R. T., and Grandhi, R. V., "Structural Shape Optimization—A Survey," *Computer Methods in Applied Mechanics and Engineering*, Vol. 57, 1986, pp. 91–106.

[20]Ding, Y., "Shape Optimization a Literature Survey," *Computers and Structures*, Vol. 24, 1986, pp. 985–1004.

[21]Bennet, J. A., and Botkin, M. E., *The Optimum Shape*, Plenum, New York, 1986.

[22]Hernandes, J. A., "Optimization of Plates and Shells Modelled with Flat Finite Elements," Ph.D. Dissertation, Civil Engineering Dept., Univ. of California, Los Angeles, 1992.

[23]Botkin, M. E., "Shape Optimization with Buckling and Stress Constraints," *AIAA Journal*, Vol. 34, No. 2, 1994, pp. 423–425.

[24]Bernadou, M., *Finite Element Methods for Thin Shell Problems*, Wiley, New York, 1996.

[25]Haftka, R. T., and Gurdal, Z., *Elements of Structural Optimization*, 3rd ed., Kluwer Academic, Norwell, MA, 1991, Sec. 6.5.

[26]Livne, E., and Milosavljevic, R., "Analytic Sensitivity and Approximation of Skin Buckling Constraints in Wing-Shape Synthesis," *Journal of Aircraft*, Vol. 32, No. 5, 1995, pp. 1102–1113.

[27]Schmit, L. A., "Structural Synthesis—Its Genesis and Development," *AIAA Journal*, Vol. 19, No. 10, 1981, pp. 1249–1263.

[28]Yang, H. T. Y., Saigal, S., and Liaw, D. G., "Advances of Thin Shell Elements and Some Applications—Version I," *Computers and Structures*, Vol. 35, No. 4, 1990, pp. 481–504.

[29]Gilewski, W., and Radwanska, M., "A Survey of Finite Element Models for the Analysis of Moderately Thick Shells," *Finite Elements in Analysis and Design*, Vol. 9, 1991, pp. 1–21.

[30]Zienkiewicz, O. C., and Taylor, R. L., *The Finite Element Method*, 4th ed., McGraw–Hill, New York, 1991.

[31]Meek, J. L., and Tan, H. S., "A Discrete Kirchhoff Plate Bending Element with Loof Nodes," *Computers and Structures*, Vol. 21, No. 6, 1985, pp. 1197–1212.

[32]Meek, J. L., and Tan, H. S., "A Faceted Shell Element with Loof Nodes," *International Journal for Numerical Methods in Engineering*, Vol. 23, 1986, pp. 49–67.

[33]Meek, J. L., and Tan, H. S., "Instability Analysis of Thin Plates and Arbitrary Shells Using Faceted Shell Element with Loof Nodes," *Computed Methods in Applied Mechanics and Engineering*, Vol. 57, 1986, pp. 143–170.

[34]Bathe, K. J., and Ho, J. W., "A Simple and Effective Element for Analysis of General Shell Structures," *Computers and Structures*, Vol. 13, 1981, pp. 673–681.

[35]Batoz, J. L., "An Explicit Formulation for an Efficient Triangular Plate Bending Element," *International Journal of Numerical Methods in Engineering*, Vol. 18, 1982, pp. 1077–1089.

[36]Dhatt, G., Marcotte, L., and Matte, Y., "A New Triangular Discrete Kirchhoff Plate/Shell Element," *International Journal for Numerical Methods in Engineering*, Vol. 23, 1986, pp. 453–470.

[37]Talbot, M., and Dhatt, G., "Three Discrete Kirchhoff Elements for Shell Analysis with Large Geometrical Non-Linearities and Bifurcation," *Engineering Computation*, Vol. 4, 1987, pp. 15–22.

[38]Stolarski, H. K., and Carpenter, N. J., "An Alternative Formulation of the Geometric Stiffness Matrix for Plate Elements," *Computers and Structures*, Vol. 24, No. 6, 1986, pp. 935–940.

[39]Farad, M., Dhatt, G., and Batoz, J. L., "A New Discrete Kirchhoff Plate/Shell Element with Updated Procedures," *Computers and Structures*, Vol. 31, No. 4, 1989, pp. 591–606.

[40]Chen, H. C., "Evaluation of Allman Triangular Membrane Element Used in General Shell Analysis," *Computers and Structures*, Vol. 43, 1992, pp. 881–887.

[41]Ertas, A., Krafcik, J. T., and Ekwaro-Osire, S., "Performance of an Anisotropic Allman/DKT 3-Node Thin Triangular Flat Shell Element," Composites Engineering, Vol. 2, 1992, pp. 269–280.

[42]Tong, P., and Rossettos, J. N., *Finite Element Method, Basic Techniques and Implementation*, MIT Press, Cambridge, MA, 1977.

[43]Felippa, C. A., "Refined Finite Element Analysis of Linear and Nonlinear Two-Dimensional Structures," Dept. of Civil Engineering, Univ. of California, Berkeley, NTIS PB-178 418, Oct. 1966.

[44]Wang, B. P., Babu, D., Nambiar, R. V., and Lawrence, K. L., "Shape Design Sensitivity Analysis Using Closed Form Stiffness Matrix for Hierarchic Triangular Elements," *Computers and Structures*, Vol. 43, No. 1, 1992, pp. 69–75.

[45]Noor, A. K., and Andersen, C. M., "Computerized Symbolic Manipulation in Structural Mechanics-Progress and Potential," *Computers and Structures*, Vol. 10, 1979, pp. 95–118.

[46]Korncoff, A. R., and Fenves, S. J., "Symbolic Generation of Finite Element Stiffness Matrices," *Computers and Structures*, Vol. 10, 1979, pp. 119–124.

[47]Beltzer, A. I., *Variational and Finite Element Methods: A Symbolic Computation Approach*, Springer–Verlag, New York, 1990.

[48]Rengarajan, G., Knight, N. F., Aminpour, M. A., "Comparison of Symbolic and Numerical Integration Methods for Assumed-Stress Hybrid Shell Element," National Technical Information Servise Order N95-13096/9INZ, 1993.

[49]Tsai, W., and Kikuchi, N., "Application of Symbolic and Algebraic Manipulation Software in Solving Applied Mechanics Problems," National Technical Information Service Order N94-13798/1INZ, 1993.

[50]Wolfram, S., *Mathematica, a System for Doing Mathematics by Computer*, Addison–Wesley, Reading, MA, 2nd ed., 1991.

[51]Halpin, J. C., *Primer on Composite Materials: Analysis*, Technomic, Westport, CT, 1984.

[52]Chia, C.-Y., *Nonlinear Analysis of Plates*, McGraw–Hill, New York, 1980.

[53]Parlett, B. N., *The Symmetric Eigenvalue Problem*, Prentice–Hall, Englewood Cliffs, NJ, 1980.

[54]Haftka, R. T., and Gurdal, Z., *Elements of Structural Optimization*, 3rd ed., Kluwer Academic, Norwell, MA, 1991, Chap. 6.

[55]Kamat, M. P., *Structural Optimization: Status and Promise*, AIAA, Washington, DC, 1993, Chaps. 12–17, 20, 21.

[56]Bisschof, C., Corliss, G., Green, L., Griewank, A., Haigler, K., and Newman, P., "Automatic Differentiation of Advanced CFD Codes for Multidisciplinary Design," *Computing Systems in Engineering*, Vol. 3, No. 6, 1992, pp. 625–637.

[57]Brockman, R. A., "Sensitivity Analysis with Plates and Shell Finite Elements," *International Journal for Numerical Methods in Engineering*, Vol. 26, 1988, pp. 1129–1143.

[58]Brockman, R. A., "Geometric Sensitivity Analysis with Isoparametric Finite Elements," *Communications in Applied Numerical Methods*, Vol. 3, 1987, pp. 495–499.

[59]Nelson, R. B., "Simplified Calculation of Eigenvector Derivatives," *AIAA Journal*, Vol. 14, No. 9, 1976, pp. 1201–1205.

[60]Shin, Y., "Analytic Shape Sensitivities and Approximations of Local and Global Airframe Buckling Constraints," Ph.D. Dissertation, Dept. of Aeronautics and Astronautics, Univ. of Washington, Seattle, WA, Oct. 1997.

[61]Bruhn, E. F., *Analysis and Design of Flight Vehicle Structures*, Tri State Offset Co., 1965, Chap. C6.

[62]Giunta, A. A., Dudley, J. M., Narducci, R., Grossman, B., Haftka, R. T., Mason, W. H., and Watson, L. T., "Noisy Aerodynamic Response and Smooth Approximations in HSCT Design," *Proceedings AIAA/NASA/USAF/ISSMO Symposium on Multidisciplinary Analysis and Optimization*, AIAA, Washington, DC, 1994.